Improved Rotor Designs of V- and Flat-type BLDC Motors Aiming at Low Torque Ripple

■

Seyed Reza Mousavi-Aghdam[1*], Amin Kholousi[2]

■

[1] Departmentof Electrical Engineering, Universityof Mohaghegh Ardabili, Ardabil, Iran
r.mousaviaghdam@uma.ac.ir
[2] Departmentof Electrical Engineering, Universityof Mohaghegh Ardabili, Ardabil, Iran
amin_kholousi@student.uma.ac.ir

■

Abstract

This paper presents modified rotor designs for two conventional V- and Flat-type BLDC motors to reduce the torque ripple. For gaining an insight into design features, the torque production characteristics are described at the beginning of the paper. By analyzing and comparing performance parameters including cogging torque, air gap flux density, back EMF, and torque average, the paper tries to describe how the torque ripple can be affected and reduced by shaping the air gap and creating specific holes in the rotor magnetic path. First, the conventional V-type BLDC motor was analyzed. Sensitivity analysis was deployed to shape the air gap and to create holes in the rotor structure. Then, all the results for both conventional and proposed V-type models were compared. Consequently, the torque ripple was effectively reduced without affecting other performance parameters. Next, the Flat-type BLDC motor was considered. Following the sensitivity analysis, the air gap was shaped, and holes were created. Similar to the proposed V-type design, the proposed Flat-type design effectively reduced the torque ripple compared with the conventional design. The results were obtained using finite element analysis; it confirmed the effectiveness of the proposed designs in both V- and Flat-type BLDC motors.

Keywords: BLDC motor, magnetic flux density, rotor structure, torque ripple, total harmonic distortion.

1. Introduction

Recently, BLDC permanent magnet motors are widely used in industries due to their excellent performance, high power and efficiency, as well as low maintenance costs. These types of motors can be divided into two categories including the internal and external rotor types. Internal rotor permanent magnet motors are classified into two categories: the interior permanent magnet (IPM) and the surface permanent magnet (SPM). In the IPM type, the permanent magnets are placed inside some holes in the rotor, while in the SPM type they are placed on the surface of the rotor. IPM motors have a very good overload capability at any speed range, while SPM motors are lacking in this capability independent of the applied current [1]. However, the construction and production of SPM motors are much simpler and easier than the IPM motors.

In applications that require low noise, minimal vibration, and high efficiency, the torque ripple is of particular interest. Also, in some exceptional cases, such as small-sized motor designs and high torque density using rare permanent magnets, the amount of torque ripple is considerable. Therefore, in recent years many investigations have been carried out on this feature to reduce the torque ripple in permanent magnet motors. The cogging torque and the interaction of back EMF and phase current waveforms are the main factors on which the torque ripple is built. Cogging torque is created by an interaction between the magnetic field produced by the permanent magnets and the stator teeth. The second factor is the profile of the back EMF, which determines the smoothness of torque production in the motor [2]. Although it may be possible to produce approximately smooth torque with any type of back EMF waveform by controlling the phase current, this will require relatively complicated control methods and costly electronic circuits. On the other side, the waveform of the back EMF is directly related to the air gap flux density. Therefore, improving air gap flux density waveforms results in back EMF with low distortion and, thus, the low torque ripple. The air gap flux is directly influenced by the rotor magnet flux density and the configuration of the stator, air gap, and rotor construction [3]. As a result, the designers try to reduce air gap flux density distortion and the back EMF harmonic distortion by making reasonable changes in the construction of the rotor and stator and also shaping the air gap in the permanent magnet motors. Much research has been conducted on reducing torque ripples in permanent magnet motors. Many studies have been carried out to reduce the torque ripple by decreasing the cogging torque via changing the arrangement of permanent magnets [4, 5], asymmetrical

designing of permanent magnets [6], making barriers and holes in the rotor [7, 8], skewing rotors and permanent magnets [9, 10] and making changes in the shape of permanent magnets [11, 12]. Research in other studies focuses on designing new controllers and drives to reduce the torque ripple. These papers discussed the torque ripple reduction in variety of ways. They include using direct power control instead of field-oriented control (FOC) and the direct torque control (DTC) [13], predicting phase currents based on back EMF using the PWM-MPC algorithm [14], using power control based on FCS-MPC [15], and using a torque control strategy considering the torque ripple caused by both non-ideal back EMF and current commutation [16]. The torque ripple reduction by improving air gap flux density profile and reducing the back EMF harmonics amplitude is discussed in [17-30]. In [17], by changing the rotor construction, high-order harmonics of back EMF and torque ripple are decreased. In [18], high-frequency acoustic vibrations and SEMF are reduced using eccentric permanent magnets. Also, in [19], torque ripple and back EMF harmonics are reduced with an asymmetrical stator design. Some changes in the type of winding distribution may reduce the harmonics of the back EMF and, thus, the torque ripple [20, 21]. Moreover, by applying some improvements in the shape of the rotor and holes, the motor performance parameters such as back EMF and torque, can be improved [22, 23]. In [24], by shaping the air gap, the flux density distortion, and the back EMF THD have been reduced; that event, in turn, mitigates the torque ripple. In [25] the design of permanent magnets considering current waveforms similar to the third harmonic injection is proposed so that the waveform of air gap flux density and torque characteristics can be improved in comparison with the conventional design. Using an advanced inverse cosine function (AICF) and an asymmetrical rotor design, the air gap flux density becomes more sinusoidal, which leads to a reduction in the torque ripple effectively [26]. Moreover, the eccentric air gap and the advanced step skewed rotor (ASSR) design may be developed and implemented to reduce the torque ripple [27]. In [28], a reduction in the torque ripple is reported by changing the barrier shape to block the circulating magnetic flux inside the rotor, making the magnetic flux pass through the air gap. Closed slots in the stator may affect the torque ripple and the rotor eddy current losses [29]. In [30], by shaping the air gap, the harmonics of no-load air gap flux density and the torque ripple have been reduced. The torque ripple analysis may be further considered in future for renewable energy systems [31].

This paper proposes modified rotor designs for two V- and Flat-type BLDC motors to reduce the torque ripple

by improving the back EMF profile. Using sensitivity analysis in two proposed designs, the air gap is shaped, and barriers are created on the rotor. Then, the analytical results of designs are extracted and, comprehensively, evaluated using FEM. The results and their comparisons have confirmed the effectiveness of the proposed designs for both V- and Flat-type BLDC topologies in terms of the torque performance. Additionally, the proposed designs have had no adverse effect on other motor performance parameters.

2. Torque Production in BLDC Motors

In BLDC motors, torque quality is determined by two factors including the cogging torque and the interaction between the back EMF and phase current waveforms. Smaller cogging torque or smaller distortions in the back EMF waveform result in a reduced torque ripple and, consequently, a better motor performance. Cogging torque can be obtained by calculating coenergy around the desired region, that is, around the edges of the magnet in proximity to the nearest tooth and slot opening as [3]

$$T_{cog} = \frac{dW_c}{d\theta} \tag{1}$$

where W_c and θ are the coenergy and the rotor mechanical position respectively. Also, the coenergy is given by

$$W_c = \int \frac{B_\theta^2}{2\mu_0} d(v_r) \tag{2}$$

where v_r stands for integral volume. Even though there

are some analytical methods to predict the cogging torque, their prediction accuracy is not sufficient to be used in a high-performance design of the motor. It is usual to employ a two-dimensional finite element analysis to examine a design for the reduced cogging torque. In that case, the Maxwell stress tensor on air gap volume can be computed to yield the cogging torque as

$$T_{cog} = \frac{L}{l_g \mu_0} \int_{S_g} r B_n B_t \, ds \tag{3}$$

where L is the active rotor length, l_g is the air gap length; r is the dummy radius; B_n and B_t are the normal and tangential flux densities of the air gap respectively. S_g is the air gap surface area. According to equation (3), the cogging torque is directly related to the active rotor length and the air gap flux density, while it is inversely related to the air gap length.

The second influential factor on the torque profile is the quality of the back EMF waveform. Equation (4) represents the electromagnetic torque produced by the motor. According to (4), the smoother peak of back EMF, along with the phase currents, which are assumed constant in the conduction interval, contributes to a lower torque ripple. Therefore, the back EMF waveform has a significant influence on the torque profile.

$$T_e = \frac{e_a i_a + e_b i_b + e_c i_c}{\omega_m} \tag{4}$$
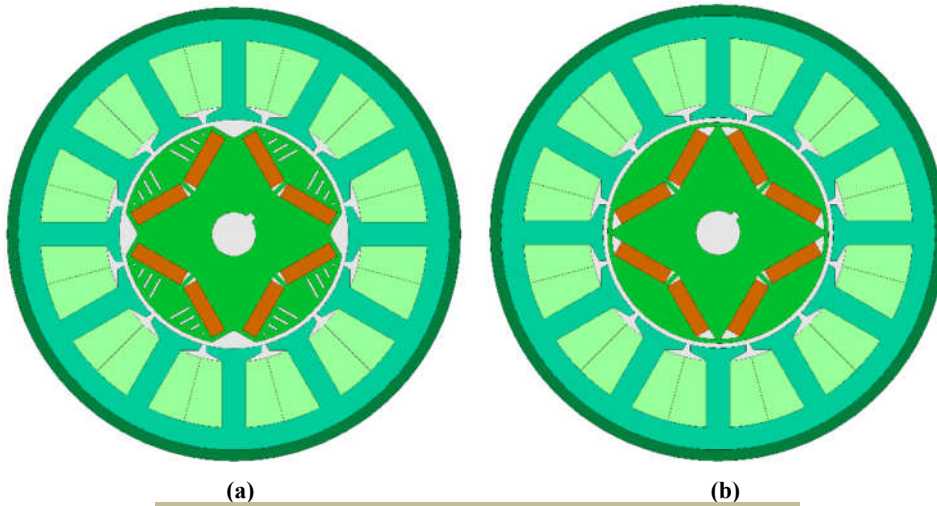

(a)   **(b)**
Fig. 1: (a) Proposed and (b) conventional V-type BLDC motors

In (4), e_a, e_b, and e_c are the phase induced back EMF voltages; i_a, i_b, and i_c are the phase currents; and ω_m is the rotor speed. Also, the induced back EMF in brushless DC motors can be calculated as in [32]

$$\begin{aligned} e &= \frac{d\lambda}{dt} = \frac{d\theta_e}{dt}\frac{d\lambda}{d\theta_e} = \omega_e \frac{d\lambda}{d\theta_e} = \frac{N_m}{2}\omega_m \frac{d\lambda}{d\theta_e} \\ &= \frac{N_m}{2}\omega_m \frac{2N\phi_g}{\pi} \end{aligned} \tag{5}$$

where N_m is the number of poles; N is the number of turns, and ϕ_g is the air gap flux. The air gap flux can also be expressed as

$$\phi_g = B_g A_g = B_g R_{ro} \theta_p L = \frac{2\pi}{N_m} B_g L R_{ro} \tag{6}$$

where θ_p is the angular pole pitch; B_g is the air gap flux density, and R_{ro} is the air gap radius. Substituting (6) into (5) yields

$$|e| = E = \frac{N_m}{2}\omega_m\frac{2N}{\pi}\left(\frac{2\pi}{N_m}B_g LR_{ro}\right) \quad (7)$$
$$= 2NB_g LR_{ro}\omega_m = K_e\omega_m$$

It can be concluded that the induced back EMF directly relates to the air gap flux density. Moreover, the air gap flux density waveform is directly affected by PM magnetic flux, rotor and stator construction as well as the shape of the air gap.

3. Proposed Designs of BLDC Motors

3.1. Proposed Design of V-Type BLDC Motors

The proposed V-type BLDC motor is shown in Figure 1 alongside the conventional one. In both designs, specifications such as the number of slots, the shape of the slots, the number of poles, the number of turns, the type of phase winding, the position, the dimensions, and magnetic characteristics of the core and permanent magnets are the same. Table 1 summarizes the common specifications of the proposed and conventional designs. As shown in Figure 1, in the proposed design, the air gap has been modified by some cuts located between two adjacent poles. Additionally, in the proposed design, there are some holes as flux barriers on the other side of the permanent magnets. These modifications improve the magnetic flux distribution in the V-type BLDC motor. To effectively design the proposed structure, the length of the cuts between the poles, the number of magnetic barriers, and the distance between the barriers will be used as design parameters. The sensitivity analysis will be conducted in the following section.

Table 1: Common specifications of the proposed and conventional V- and Flat-type designs

Parameter	Value	Material
Stator external diameter	100mm	Cognet M470
Stator internal diameter	52mm	
Rotor diameter	50mm	Cognet M470
Remanence of PMs	1.2T	NdFeB N35
Stack length	70mm	-
Air gap length	1mm	-
Slot numbers	12	-
Pole numbers	4	-
Rated power	350 W	-
Rated voltage	80 V	-

3.1.1. Simulation and Meshing Characteristics

Figure 2 illustrates the meshing of both proposed and conventional designs. In areas with high gradients such as air gaps, the mesh density should be set properly. Otherwise, the results will not be accurate. As shown in the figure, in both proposed and conventional designs, the mesh density in the air gap is higher than in other areas but

lower in areas such as slots and stator back iron. Simulations are also conducted in the transient magnet mode, and the results have been analyzed.

(a)

(b)
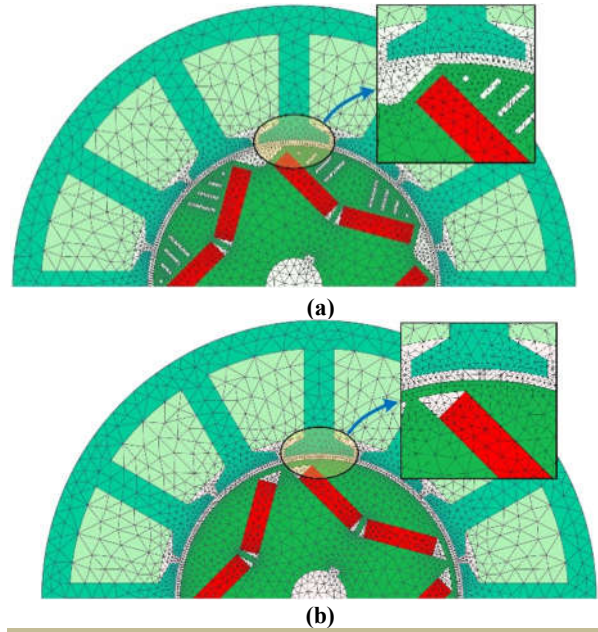
Fig. 2: Illustrations of meshing in both (a) proposed and (b) conventional V-type designs.

3.1.2. Sensitivity Analysis of the Proposed V-Type BLDC Motor

This section uses sensitivity analysis to determine the most optimal values for the air gap shaping design parameter. As shown in Figure 3a, L indicates the length of the cuts between the poles. L is changed in ten steps, and the results are then compared. Considering nominal running conditions, torque waveforms are calculated in one period and are shown in Figure 3b for different values of L. As seen, by increasing the length, L, the average value of the torque increases for the first steps and remains constant. Thus, there may be a maximum optimal value for the design parameter, L. The same goes for the torque ripple, inversely, by increasing the length, L.

Based on Figure 3b and comparing the last two cases, IX and X, it can be seen that the design parameter in case X has reached its optimal value beyond which the average torque and the torque ripple cannot be changed further. Therefore, state X is selected and fixed in the following sensitivity analysis for the flux barriers.

In the next step, according to Figure 4, the sensitivity analysis is performed to determine effectively the number and distances between the barriers on the outer side of the permanent magnets. These barriers confine the flux produced by the permanent magnet into an air gap suitably and prevent it from circulating considerably.
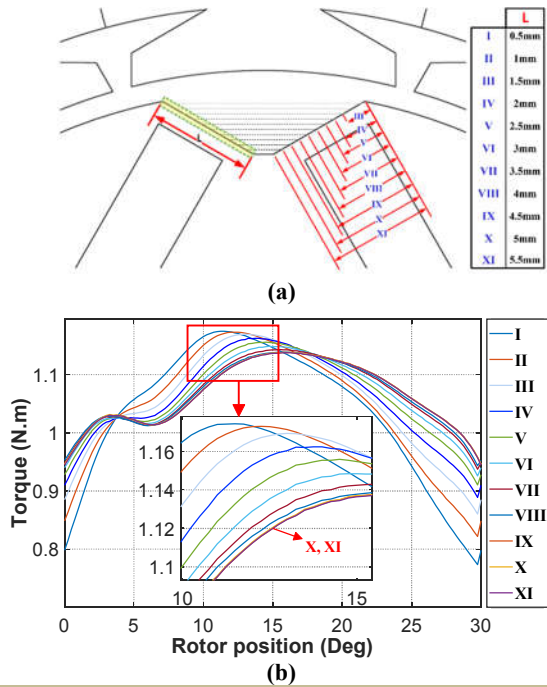
Fig. 3: (a) Geometrical states and (b) the motor total torque waveforms in terms of design parameter, L.

The distances specified in blue, as shown in Figure 4, are fixed in any step of sensitivity analysis and have the same size. For any specific number of flux barriers, the distance between barriers is changed, and the results are, then, compared. In the first step, the distance, as shown in Figure 4a, is changed for two flux barriers. In the second step, the distance between the holes, as shown in Figure 4b, is changed for three flux barriers. Finally, in the third step, the distance, according to Figure 4c, is modified for four barriers. The established torques, in these three steps, are compared with each other, and the 4-hole design with a distance of 1.75 mm from each other is selected for flux barriers; it has a higher value of average torque than the others. The torque waveform in one cycle for the selected design is shown in Figure 4d.

3.1.3. Analysis and Result Comparisons of the Conventional and Proposed V-type BLDC Motors

In this section, the performance results and waveforms of different analyses for the proposed and conventional V-type BLDC motors are presented and compared in the same conditions. First, the distributions of flux lines in the two proposed and conventional designs are compared. Figure 5 depicts the flux lines passing through the rotor and stator when the minimum and maximum values of the torque applied to the rotor. Also, the active phases in each mode are specified. The flux barriers in the structure of the proposed V-type rotor change the flux path near the air gap and may affect the magnetic field stress in some rotor angles.
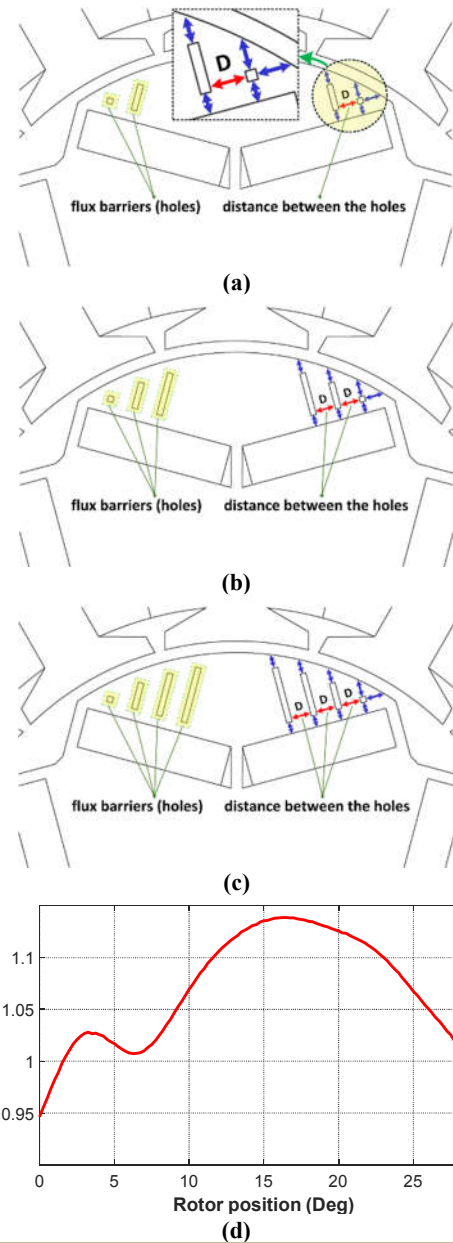

Fig. 4: Geometrical view of the proposed V-type BLDC motor with (a) two, (b) three, and (c) four flux barriers considering the distance, D, between them and (d) selected design torque waveform

Next, in order to compare the two proposed and conventional V-type designs comprehensively, the magnetic flux density in all parts of the motor is also examined. Figure 6 shows the flux density for the minimum and maximum torques in the proposed and conventional V- type motors. The active phases are also specified in each case. The stator in both designs experiences approximately the same flux ensities, but in the rotor, there are some differences near the air gap. Moreover, the maximum magnetic flux density of the stator is selected to be near the knee point of the core magnetic curve.
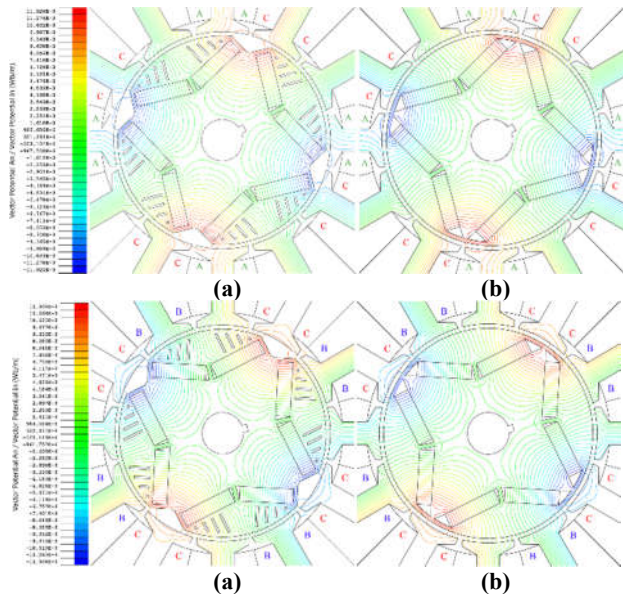
Fig. 5: Flux lines distribution when applying (a) - (b) the maximum, and (c) - (d) minimum torque to the rotor of the proposed and conventional V-type BLDC motors.
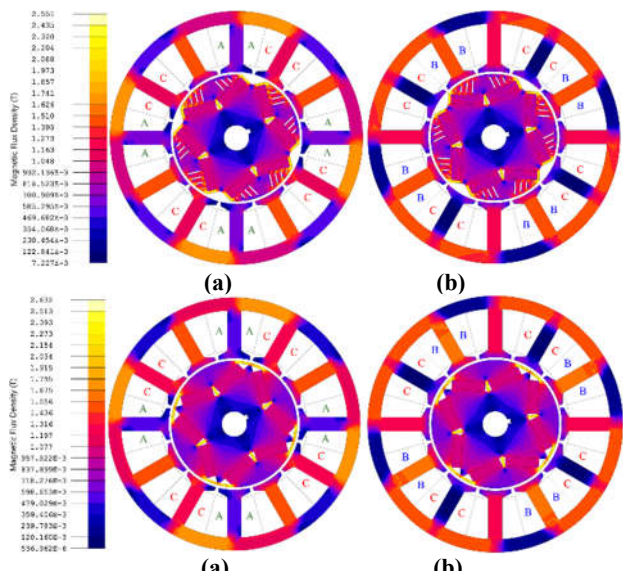
Fig. 6: Magnetic flux density of the proposed and conventional motors in the (a,c) maximum and (b,d) minimum torque modes

Figure 7 shows the air gap flux density waveforms for the proposed and conventional V-type designs. Figure 7a shows the normal components of the air gap flux density in both motors, which seems to be almost the same. However, as shown in Figure 7b, the tangential components of the air gap flux density are different. As it can be seen, the slotting effect in the aforementioned components of the proposed design is significantly less than that of the conventional one. Therefore, the difference in the tangential air gap flux density waveforms of the proposed and conventional design leads to different back EMFs. Consequently, the back EMF waveform influences the torque ripple which has less value in the proposed design.
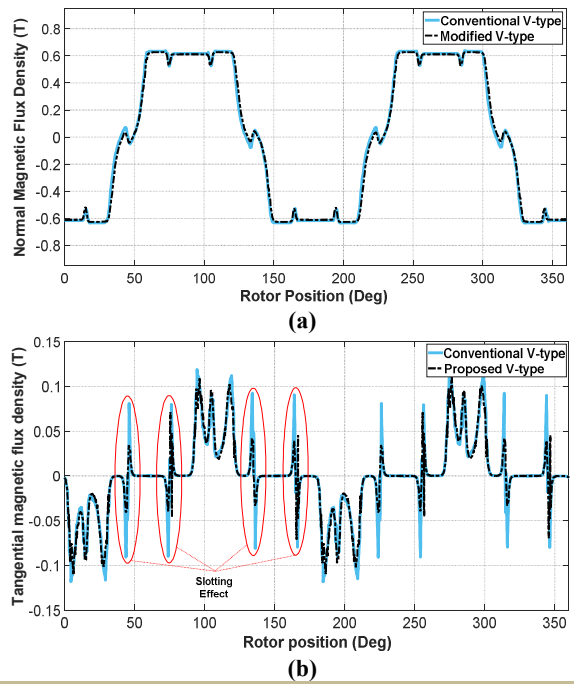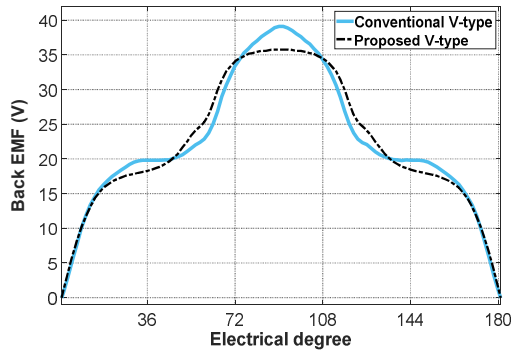

Fig. 7: (a) Normal and (b) tangential air gap flux density waveforms for the proposed and conventional V-type BLDC motors

Figure 8 shows the back EMF waveforms of the conventional and proposed V-type motors. For similar working conditions, the back EMF waveform of the proposed design is smoother than the conventional one. The THD, 14.14% for the proposed design and 17.52% for the conventional design, indicates 19.29% reduction in the total harmonic distortion of the proposed design. Of course, all of the back EMF values in one period are not involved in the torque production because of the phase commutation.

The cogging torque is also analyzed for two conventional and proposed V-type motors, as shown in Figure 9. As seen, the cogging torque in the proposed design is slightly higher than the conventional one. However, this difference does not have an undesirable effect on the total torque ripple.
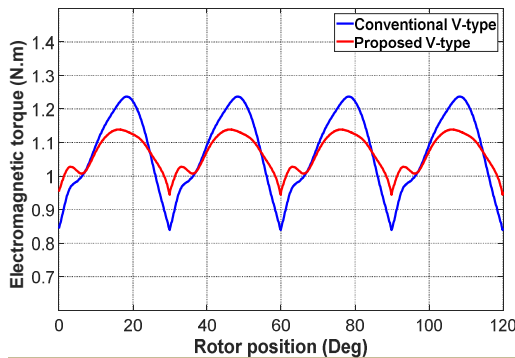
Figure 10 shows the total electromagnetic torque in the proposed and conventional V-type designs for the rated phase currents. As shown, the torque ripple in the proposed design with 5.13 percent is less than the conventional one with 11.03 percent. This issue indicates a 53.49% reduction in the torque ripple for the proposed design compared with the conventional one. Average torques, in the proposed and conventional designs, are 1.066 N.m and 1.071 N.m respectively. As a result, the toque ripple reduction in the proposed design has been obtained without any considerable change in the average torque.

Fig. 8: Comparison of the induced back EMF for the proposed and conventional V-type BLDC motors
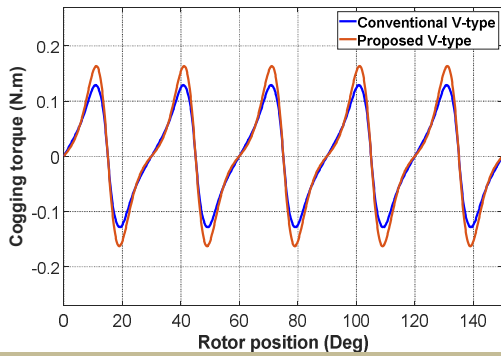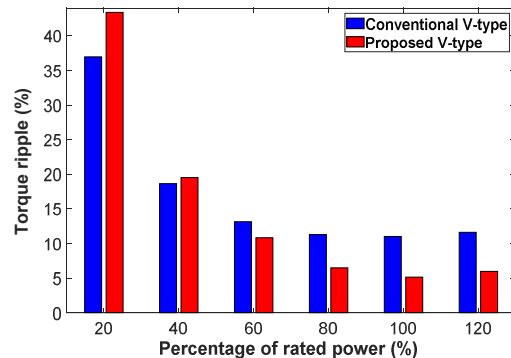

Fig. 9: Comparison of the cogging torque for the proposed and conventional V-type BLDC motors

Figure 11 shows the torque ripple for different output powers in both conventional and proposed V-type BLDCs. For each different output power, the average torque is constant for both BLDC motors. On the other side, the torque ripple in the proposed design is less than the conventional one for the outputs near the rated power. For example, for 120% of the rated output, the torque ripple is 5.96% in the proposed design and 11.6% in the conventional design. These values for the rated output are about 5.13% and 11.03% respectively. These values for 80% of the rated output are 11.27% in the conventional design and 6.50% in the proposed one.

In order to finalize the comparison between different proposed and conventional V-type designs, the ripple and average value of the torque are further analyzed based on different PM materials of the rotor and various output power. Figure 12 and figure 13 show the torque ripple and its average value for both designs. Figure 12a and 12b depict the torque ripple for the proposed and conventional designs respectively. As it can be seen, the torque ripple of the proposed design, while using PMs with high remanent flux density,

Fig. 10: Electromagnetic torque waveforms of the proposed and conventional V-type BLDC motors

Fig. 11: Torque ripple for different output powers in the proposed and conventional V-type BLDC motors

(a)

(b)
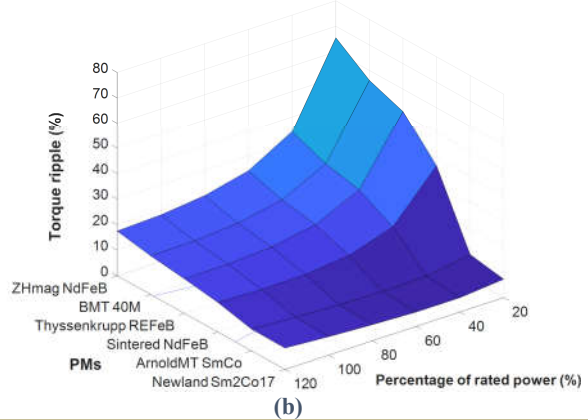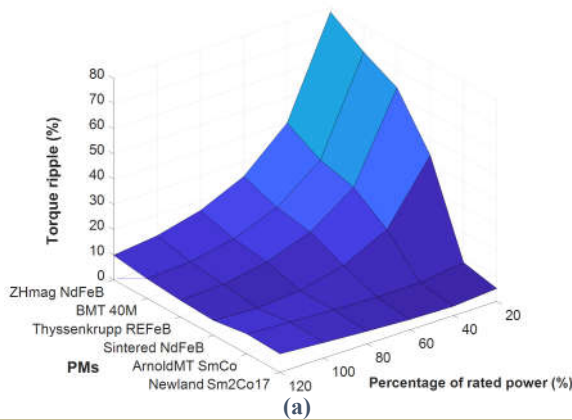
Fig. 12: Illustration of the torque ripple for the (a) proposed and (b) conventional V-type BLDC motors considering different PM materials and various output powers.
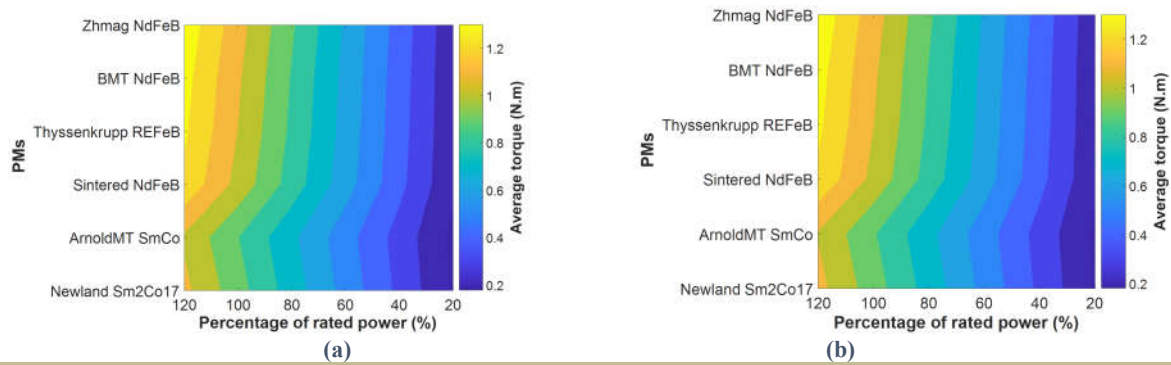
Fig. 13: Illustration of the mean value of the torque for (a) proposed and (b) conventional V-type BLDC motors considering different PM materials and various output powers

is considerably less than the conventional one near the rated output power. Also, the torque ripple, while using PMs such as SmCo, is slightly lower than the conventional design. Figure 13a and 13b show the average value of the torque for proposed and conventional designs respectively. It can be clearly seen that the average value of the torque is almost the same for both designs. As a result, the proposed V-type design is very suitable for the applications requiring high torque density and low torque ripple.

3.2. Proposed Design of Flat-Type BLDC Motors
Figure 14 shows the proposed Flat-type BLDC motors compared to the conventional ones. In both designs, parameters including the number of turns, the type of phase winding, the position, dimensions, and the magnetic characteristics of the permanent magnets are the same. Moreover, the stator characteristics including the number of stator teeth, the shape of the slots, and the core magnetic characteristics are the same.
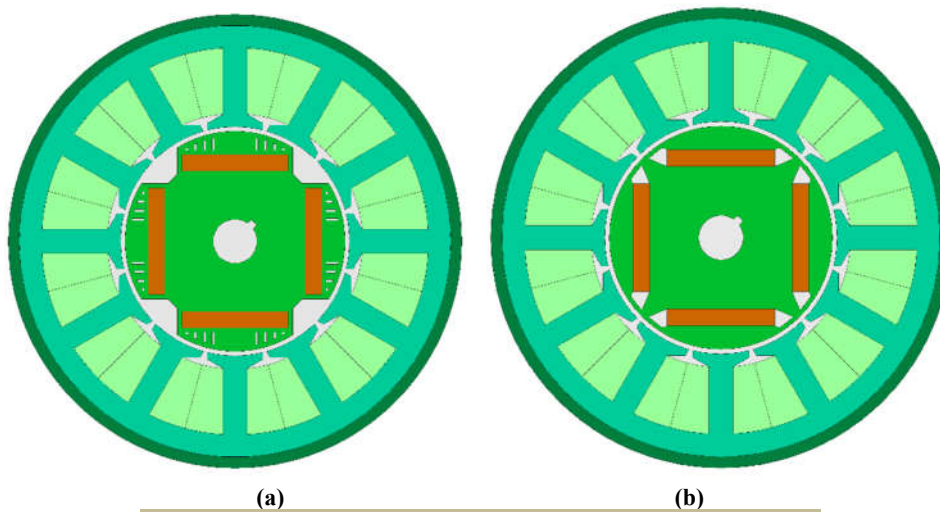

Fig. 14: (a) Proposed and (b) conventional Flat-type BLDC motors

Table 1 summarizes the common specifications of the proposed and conventional designs. As shown in Figure 14, in the proposed design the air gap has been modified by some cuts located between two adjacent poles. Additionally, in the proposed design, there are some holes as flux barriers on the other side of the permanent magnets. These modifications improve magnetic flux distribution in the proposed Flat-type BLDC motor. To design the proposed structure effectively, the length of the cuts between the poles, the number of the holes as magnetic barriers, and the distance between the holes are selected as the design parameters. These are further

evaluated using sensitivity analysis in the following section.

3.2.1. Simulation and Mesh Characteristics
Figure 15 illustrates the meshing of both proposed and conventional designs. In areas with high gradients such as air gaps, the mesh density should be set properly. Otherwise, the results will not be accurate. As shown in the figure, in both proposed and conventional designs, the mesh density in the air gap is higher than that in other areas but lower in areas such as slots and stator back iron. Simulations are also conducted in the transient magnet mode, and the results have been analyzed.

3.2.2. Sensitivity Analysis of the Proposed Flat-Type BLDC Motors

This section uses sensitivity analysis to determine the most optimal values for the air gap shaping design parameters in the proposed Flat-type structure. As shown in Figure 16a, L indicates the length of the cuts between the poles. L is changed in ten steps, and the results are, then, compared. Considering nominal conditions, back EMF waveforms are shown in Figure 16b for different values of L. As seen, by increasing the length, L, the back EMF increases first and remains constant. Also, Figure 16c shows torque waveforms in one period for different values of L. As seen, by increasing the length, L, the average value of the torque increases for the first steps and remains constant for the subsequent steps. Consequently, the design parameter, L, may have an optimal value. The same goes for the torque ripple, inversely, by increasing the length, L.
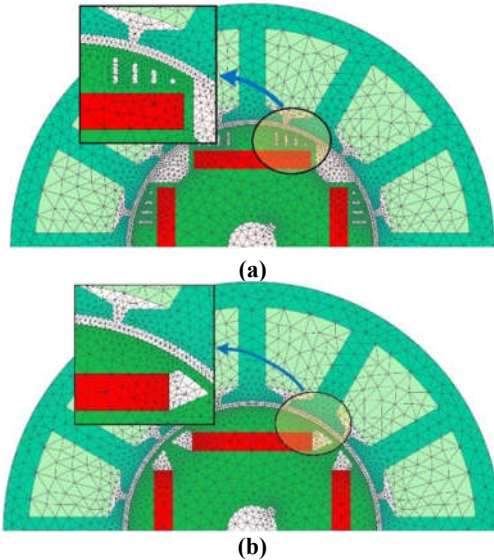

(a)

(b)

Fig. 15: Illustrations of meshing in both (a) proposed and (b) conventional Flat-type designs

Figure 16c shows that by comparing the last three states, IX, X, and XI, one can observe that the design parameter in state XI has reached its optimal value. Beyond this value, the back EMF, torque ripple, and average torque value cannot be changed further. Therefore, the state XI is selected and fixed in the following sensitivity analysis for the flux barriers.
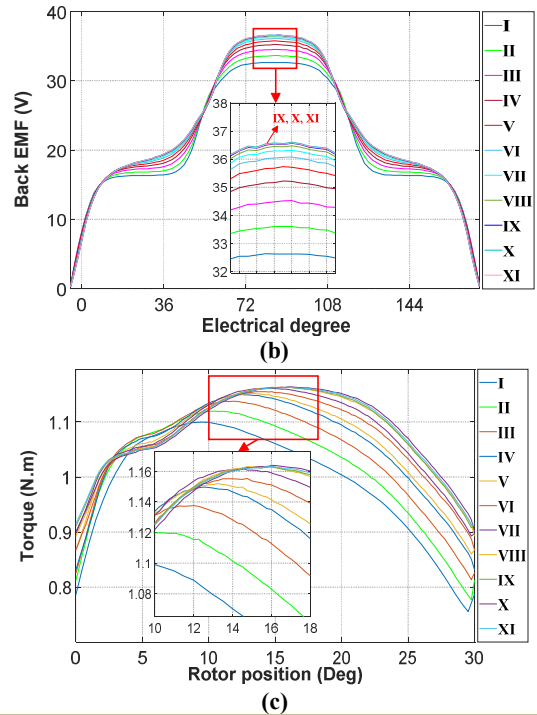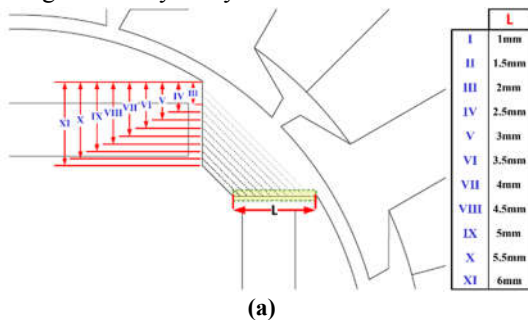

(a)

(b)

(c)

Fig. 16: (a) Geometrical states, (b) induced back EMF, and (c) the motor torque waveforms in terms of design parameter, L, for the proposed Flat-type design

In the next step, according to Figure 17, the sensitivity analysis is performed to determine effectively the number and distances between the barriers on the outer side of the permanent magnets. These barriers confine the flux produced by the permanent magnet into the air gap suitably and prevent it from circulating considerably.

The distances specified in blue, as shown in Figure 17, are fixed in any step of sensitivity analysis and have the same size. For any specific number of flux barriers, the distance between barriers is changed, and the results are, then, compared. In the first step, shown in Figure 17a, the distance is changed for two flux barriers. In the second step, shown in Figure 17b, the distance between the holes is changed for three flux barriers. Finally, in the third step, according to Figure 17c, the distance is modified for four barriers. The established torques, in these three steps, are compared with each other, and a 4-hole design with a distance of 1.5 mm from each other is selected as the flux barrier design with the highest average torque value. The torque waveform in one cycle for the selected design is shown in Figure 17d.

(a)

(b)

(c)

(d)
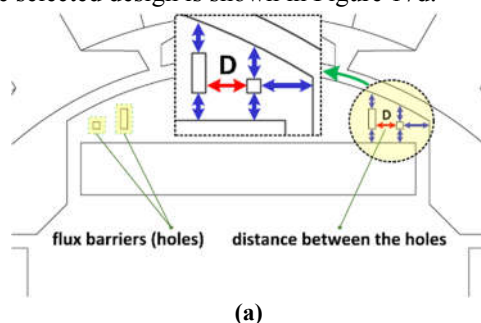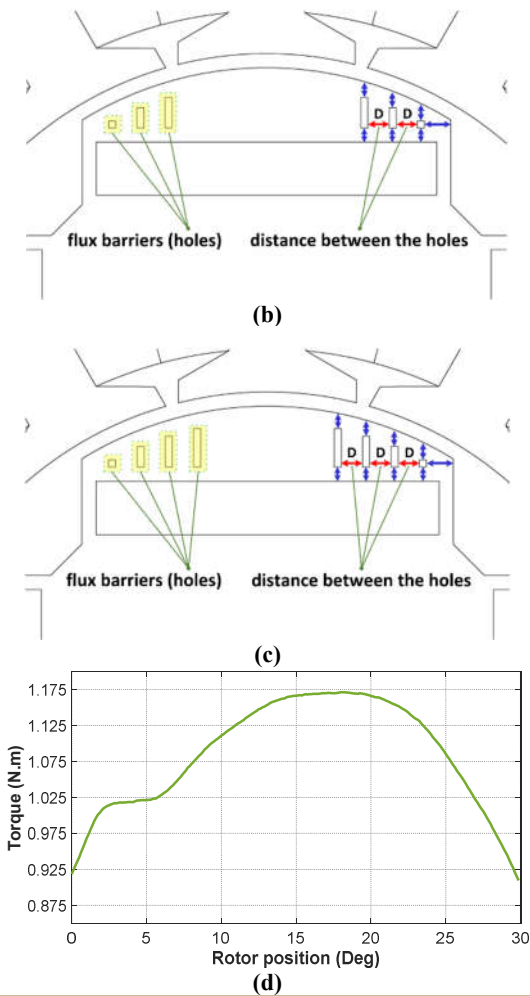
Fig. 17: Geometrical view of the proposed Flat-type BLDC motor with (a) two, (b) three, (c) four flux barriers and the distance, D, between them and(d) selected design torque waveform
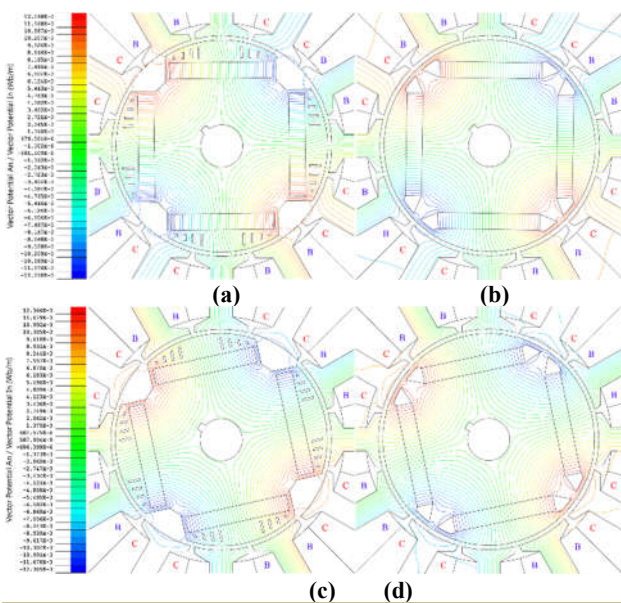

Fig. 18: Flux lines distribution when applying (a) - (b) the maximum, and (c) - (d) minimum torque to the rotor of the proposed and conventional V-type BLDC motors

3.2.3. Analysis and Result comparisons of the Conventional and Proposed Flat-Type BLDC Motors

In this section, the performance results and waveforms of different analyses for the proposed and conventional Flat-type BLDC motors are presented and compared in the same conditions. First, the distributions of flux lines in two proposed and conventional designs are compared. Figure 18 depicts the flux lines passing through the rotor and stator when the minimum and maximum values of the torque are applied to the rotor. Also, the active phases in each mode are specified. The flux barriers in the structure of the proposed Flat-type rotor change the flux path near the air gap and may affect the magnetic field stress in some rotor angles.

Next, in order to make a reasonable comparison between both proposed and conventional Flat-type designs, the magnetic flux density in all parts of the motor is also examined. Figure 19 shows the flux density for the minimum and maximum torques in the proposed and conventional Flat-type motors. Active phases are also specified in each case. The stator in both designs approximately experiences the same flux densities, but in the rotor, there are some differences near the air gap. Moreover, the maximum magnetic flux density of the stator is selected to be near the knee point of the core magnetic curve.
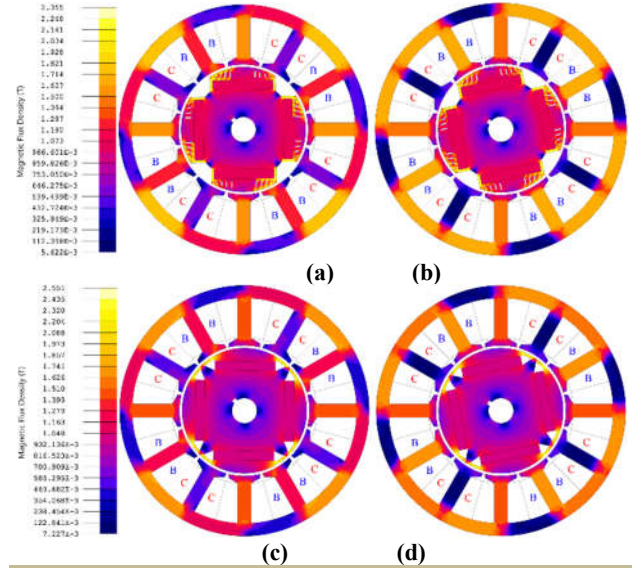
Fig. 19: Magnetic flux density of the proposed and conventional motors in the (a,c) maximum and (b,d) minimum torque modes

Figure 20 shows the air gap flux density waveforms for the proposed and conventional Flat-type designs. Figure 20a shows the normal components of the air gap flux density in both motors, which seems to be almost the same. However, as shown in Figure 20b, the tangential components of the air gap flux density are different. As seen, the slotting effect in the mentioned components of

the proposed design is significantly less than the conventional one. Therefore, the difference in the tangential air gap flux density waveforms of the proposed and conventional design leads to different back EMFs. Consequently, the back EMF waveform influences the torque ripple, which has less value in the proposed design.

Figure 21 shows the back EMF waveforms of the conventional and proposed Flat-type motors. For a similar working condition, the back EMF waveform of the proposed design is smoother than the conventional one. The THD is 15.29% for the proposed design and 18.97% for the conventional design. It indicates 19.39% reduction in the total harmonic distortion of the proposed design. Of course, all of the back EMF values in one period are not involved in the torque production because of the phase commutation.
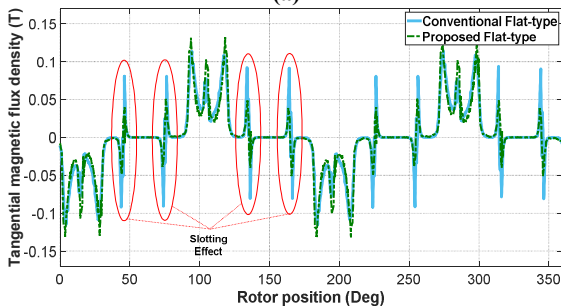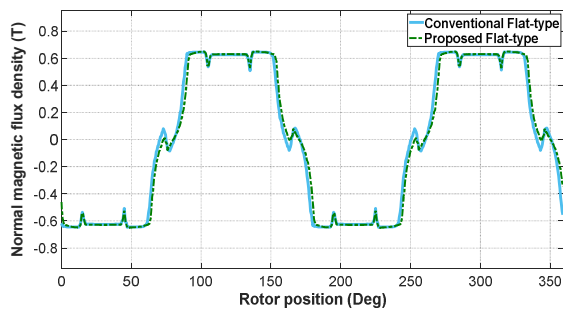
The cogging torque is also analyzed for two conventional and proposed Flat-type motors and is shown in Figure 22. As seen, the cogging torque in the proposed design is slightly higher than the conventional one. However, this difference does not have an undesirable effects on the total torque ripple.

Fig. 22: Comparison of the cogging torque for the proposed and conventional Flat-type BLDC motors
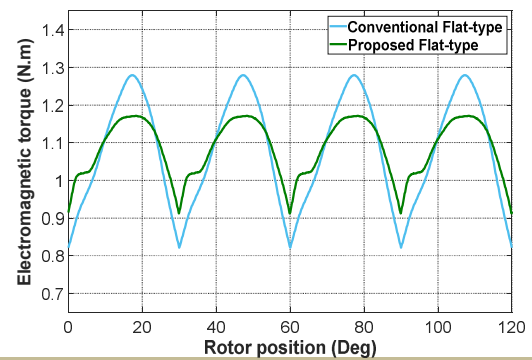
11

Fig. 23: Electromagnetic torque waveforms of the proposed and conventional Flat-type BLDC motors

10

(a)

(b)

Fig. 20: (a) Normal and (b) tangential air gap flux density waveforms for the proposed and conventional V-type BLDC motors

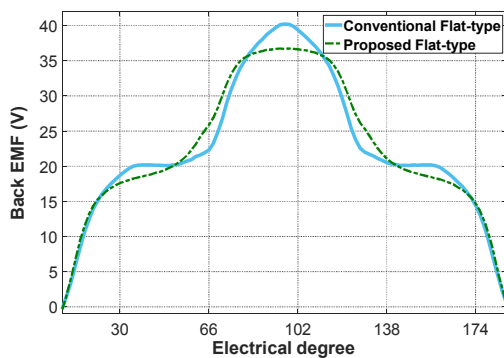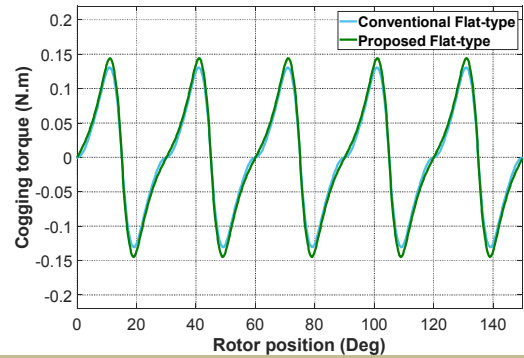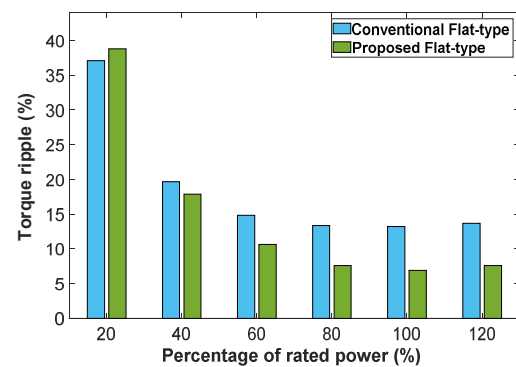**Fig. 24: Torque ripple for different output powers in the proposed and conventional Flat-type BLDC motors.**

Figure 23 shows the total electromagnetic torque in the proposed and conventional Flat-type designs for the rated phase currents. As shown, the torque ripple in the proposed design, with 6.91 percent, is less than the conventional one with 13.20 percent. This indicates a 47.65% reduction in the torque ripple for the proposed design compared with the conventional one. The average torques in the proposed and conventional designs are 1.085 N.m and 1.079 N.m respectively. As a result, the toque ripple reduction in the

Fig. 21: Comparison of the back EMF for the proposed and conventional Flat-type BLDC motors.

proposed design has been obtained without considerable change in the average torque.

Figure 24 shows the torque ripple for different output power in both conventional and proposed Flat-type BLDCs. The average value of the torque for each different output power in terms of phase currents is constant in both BLDC motors. On the other side, the torque ripple in the proposed design is less than the conventional one for the outputs near the rated power. For example, for 120% of the rated output, the torque ripple is 7.26% in the proposed and 1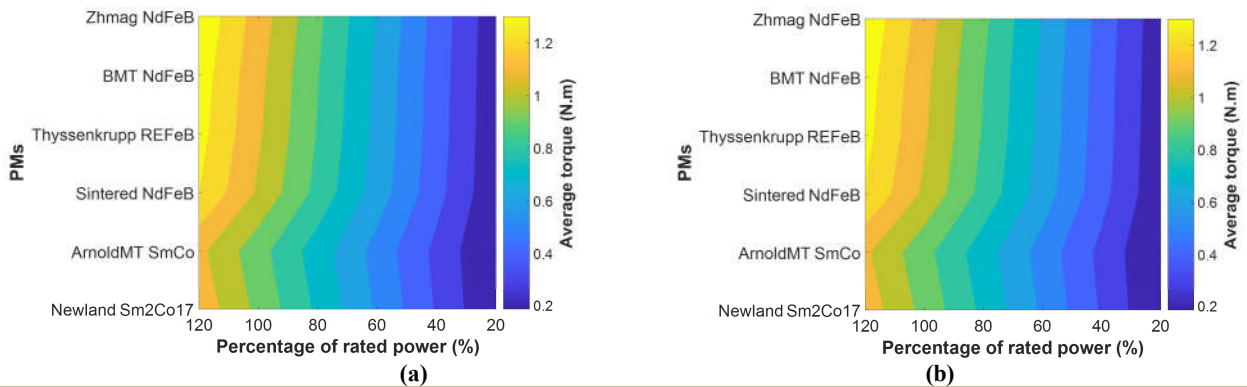3.70% in the conventional designs. These values for the rated output are about 6.91% and 13.20% respectively. For 80% of the rated power, the conventional design has a ripple of 13.34%, and the proposed design has a ripple of 7.61%.
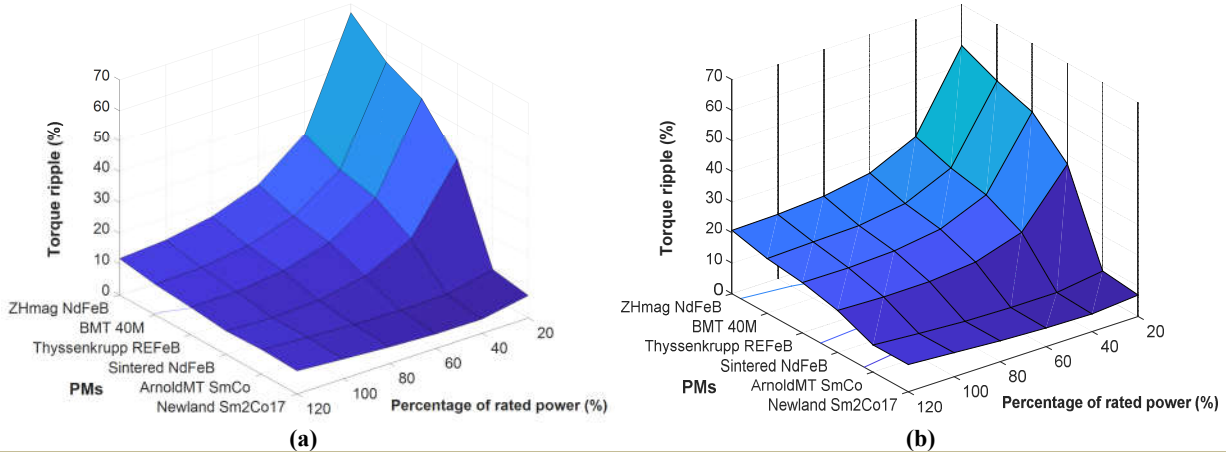
Fig. 25: Torque Ripple of the (a) proposed and (b) conventional Flat-type BLDC motors dependent on different PM materials and various output powers

Fig. 26: Average torque value for (a) proposed and (b) conventional Flat-type BLDC motors dependent on different PM materials and various output powers

In order to finalize the comparison between different proposed and conventional Flat-type designs, the ripple and average torque values are further analyzed based on different PM materials of the rotor and various output power. Figure 25 and figure 26 show the torque ripple and its average value for both designs. Figure 25a and 25b depict the torque ripple for the proposed and conventional designs respectively. As seen, the torque ripple of the proposed design, while using PMs with high remanent flux density, is considerably less than the conventional one near rated output power. Also, while using PMs such as SmCo, the torque ripple is slightly lower than the conventional design. Figure 26a and 26b show the average value of the torque for the proposed and conventional designs respectively. It can clearly be seen that the average value of the torque is almost the same for both designs. As a result, the proposed Flat-type design is very suitable for the applications requiring high torque density and the low torque ripple.

Table 2 summarizes the results obtained from the conventional and proposed V- and Flat-type BLDC motors. Based on Table 2, both proposed designs have lower torque ripple than the conventional ones with the same stator structure and magnetic materials. Furthermore, the improvement of the torque ripple has reached without adverse effect on the other performance characteristics such as average torque.

Table 2: Torque performance comparison of the proposed and conventional designs

	Torque Ripple	Torque Average
Conventional V-type model	11.03%	1.071 N.m
Proposed V-type model	5.13%	1.066 N.m
Conventional Flat-type model	13.20%	1.079 N.m
Proposed Flat-type model	6.91%	1.085 N.m

4. Conclusion

In this paper, two conventional V- and Flat-type BLDC motors have thoroughly been investigated to reduce electromagnetic torque ripple. Optimized rotor structures are proposed for both types of BLDCs, in which the air gap shape is modified, and holes are created as flux barriers. Comprehensive evaluations are carried out using a finite element method to investigate the suitability and the performance of the proposed V- and Flat-type structures. By reviewing and examining the evaluations, it is clear that the slotting effect on the air gap flux density is reduced, and the back EMF profile is improved. The results confirm the effectiveness of the proposed designs in reducing the torque ripple. The proposed and conventional V-type designs have torque ripples of 5.13% and 11.03% respectively, indicating a 53.49% reduction in the ripple of the proposed structure. Similarly, the torque ripples for the proposed and conventional flat-type designs are 6.91% and 13.20% respectively, indicating a 47.65% reduction in the ripple. Considering the reduction of the torque ripples, the mean value of the torque is almost the same in both designs. Many optimization algorithms may be used to improve the torque ripple further and could be proposed as a future work. As a result, the proposed rotor structures are suitable candidates for applications requiring low torque ripple.

References

[1] Vagati, A., Pellegrino, G., Guglielmi, P., "*Comparison between SPM and IPM motor drives for EV application*", The XIX International Conference on Electrical Machines - ICEM 2010, Rome, Italy, 2010, pp. 1-6, doi:10.1109/ICELMACH.2010.5607911.

[2] Sumega, M., Zossak, S., Varecha, P., Rafajdus, P., "*Sources of torque ripple and their influence in BLDC motor drives*", Transportation Research Procedia, the 13th International Scientific Conference on Sustainable, Modern and Safe Transport, 2019, pp. 519-526, doi:10.1016/j.trpro.2019.07.075.

[3] Krishnan, R., "Permanent magnet synchronous and brushless DC motor drives", Blacksburg, Virginia, USA: Taylor & Francis Group, 2010, doi:10.1201/9781420014235.

[4] Yoon K., Kwon, B., "*Optimal Design of a New Interior Permanent Magnet Motor Using a Flared-Shape Arrangement of Ferrite Magnets*", IEEE Trans. Magn., Vol. 52, pp. 1-4, Jul. 2016, doi:10.1109/TMAG.2016.2524505.

[5] Tudorache, T., Trifu, I., "*Permanent-magnet synchronous machine cogging torque reduction using a hybrid model*", IEEE Trans. Magn., Vol. 48, pp. 2627–2632, Oct. 2012, doi:10.1109/TMAG.2012.2198485.

[6] Ren, W., Xu, Q., Li, Q., "*Reduction of cogging torque and torque ripple in interior PM machines with asymmetrical V-type rotor design*", IEEE Trans. Magn., Vol. 52, pp. 1-5, Jul. 2016, doi:10.1109/TMAG.2016.2530840.

[7] Kang, G., Son, Y., Kim, G., Hur, J., "*A novel cogging torque reduction method for interior-type permanent-magnet motor*", IEEE Trans. Ind. Appl., Vol. 45, pp. 119-125, Jan/Feb. 2009, doi:10.1109/TIA.2008.2009662.

[8] Mousavi-Aghdam, S. R., Kholousi, A., "*Design and analysis of a new topology of rotor magnets in brushless DC motors to reduce cogging torque*", International Journal of Industrial Electronics Control and Optimization, Vol. 4, pp. 77-86, Jan. 2021, doi:10.22111/ieco.2020.34565.1282.

[9] Fei, W., Zhu, Z. Q., "*Comparison of cogging torque reduction in permanent magnet brushless machines by conventional and herringbone skewing techniques*", IEEE Trans. Energy Convers., Vol. 28, pp. 664-674, Sep. 2013, doi:10.1109/TEC.2013.2270871.

[10] Zhao, W., Lipo, T.A., Kwon, B., "*Torque pulsation minimization in spoke-type interior permanent magnet motors with skewing and sinusoidal permanent magnet configuration*s", IEEE Trans. Magn., Vol. 51, pp.1-4, Nov. 2015, doi:10.1109/TMAG.2015.2442977.

[11] Chen, N., Ho, S. L., Fu, W. N., "*Optimization of permanent magnet surface shapes of electric motors for minimization of cogging torque using FEM*", IEEE Trans. Magn., Vol. 46, pp. 2478–2481, Jun. 2010, doi:10.1109/TMAG.2010.2044764.

[12] Zhou, M., Zhang, X., Zhao, W., Ji, J., Hu, J., "*Influence of magnet shape on the cogging torque of a surface-mounted permanent magnet motor*", Chinese Journal of Electrical Engineering, Vol. 5, pp. 40-50, Dec. 2019, doi:10.23919/CJEE.2019.000026.

[13] Allan G. de Castro, et al., "*Improved finite control-set model-based direct power control of BLDC motor with reduced torque ripple*", IEEE Trans. Ind. Appl., Vol. 54, pp. 4476–4484, Sep./Oct. 2018, doi:10.1109/TIA.2018.2835394.

[14] Xia, K., Ye, Y., Ni, J., Wang, Y., Xu, P., "*Model predictive control method of torque ripple reduction for BLDC moto*r", IEEE Trans. Magn. , Vol. 56, pp. 1-6, Jan.

2020, doi:10.1109/TMAG.2019.2950953.

[15]   Castro, A. G.,et al., "*Finite control-set predictive power control of BLDC drive for torque ripple reduction*", IEEE Latin America Transactions, Vol. 16, pp. 1128-1135, Apr. 2018, doi:10.1109/TLA.2018.8362147.

[16]   Shi, T., Cao, Y., Jiang, G., Li, X., Xia, C., "*A torque control strategy for torque ripple reduction of brushless DC motor with non-ideal back electromotive force*", IEEE Trans. Ind. Electron. Vol. 64, pp. 4423-4433, Jun. 2017, doi:10.1109/TIE.2017.2674587.

[17]   Lee, J. H. , Kim, D. H. , Park, I. H., "*Minimization of higher back-EMF harmonics in permanent magnet motor using shape design sensitivity with B-spline parameterization*", IEEE Trans. Magn., Vol. 39, pp. 1269-1272, May. 2003, doi:10.1109/TMAG.2003.810162.

[18]   Liu, T., Zhao, W., Ji, J., Zhu, Sh., Cao, D., "*Effects of eccentric magnet on high-frequency vibroacoustic performance in integral-slot SPM machines*", IEEE Trans. Energy Convers., Vol. 36, pp. 2393-2403, Sept. 2021, doi:10.1109/TEC.2021.3060752.

[19]   Kim, H., Kim, Y.J., Jung, S.Y., "*Torque ripple and back EMF harmonic reduction of IPMSM with asymmetrical stator desig*n", in Electrical Machines and Systems (ICEMS), 2017 20th International Conference on. IEEE. 2017, pp. 1-4, doi:10.1109/ICEMS.2017.8056477.

[20]   Hua, W., Zhu, X., Wu, Z., "*Influence of coil pitch and stator-slot/rotor-pole combination on back EMF harmonics in flux-reversal permanent magnet machines*", IEEE Trans. Energy Convers., Vol. 33, pp. 1330–1341, Sep. 2018, doi:10.1109/TEC.2018.2795000.

[21]   Li, F., Wang, K., Li, J., Zhang, H. J., "*Suppression of even-order harmonics and torque ripple in outer rotor consequent-pole PM machine by multilayer winding*", IEEE Trans. Magn., Vol. 54, pp. 1-5, Jun. 2018, doi:10.1109/TMAG.2018.2839740.

[22]   Seo, U. J., Chun, Y.D., Choi, J.H., Han, P.W., Koo, D. H., Lee, J., "*A technique of torque ripple reduction in interior permanent magnet synchronous motor*", IEEE Trans. Magn., Vol. 47, pp. 3240-3243, Oct. 2011, doi:10.1109/TMAG.2011.2150742.

[23]   Kim, K. Ch., Koo, D. H., Hong, J. P., Lee, J., "*A Study on the Characteristics Due to Pole-Arc to Pole-Pitch Ratio and Saliency to Improve Torque Performance of IPMS*M", IEEE Trans. Magn., Vol. 43, pp. 2516-2518, Jun. 2007, doi:10.1109/TMAG.2007.893524.

[24]   Lee, S., Kim, Y. J., Jung, S. Y., "*Numerical investigation on torque harmonics reduction of interior PM synchronous motor with concentrated winding*", IEEE Trans. Magn., Vol. 48, pp. 927-930, Feb. 2012, doi:10.1109/TMAG.2011.2174346.

[25]   Wang, K., Zhu, Z. Q., Ombach, G., "*Torque improvement of five-phase surface-mounted permanent magnet machine using third-order harmoni*c", IEEE Trans. Energy Convers., Vol. 29, pp. 735-747 , Sep. 2014, doi:10.1109/TEC.2014.2326521.

[26]   Jung, Y. H., Lim, M. S., Yoon, M. H., Jeong, J. S., Hong, J. P., "*Torque ripple reduction of IPMSM applying asymmetric rotor shape under certain load condition*",

IEEE Trans. Energy Convers., Vol. 33, pp. 333–340, Mar. 2018, doi:10.1109/TEC.2017.2752753.

[27]   Chen, W., Ma, J., Wu, G., Fang, Y., "*Torque ripple reduction of a salient-pole permanent magnet synchronous machine with an advanced step-skewed rotor des*ign", IEEE Access, Vol. 8, pp. 118989–118999, Jun 2020, doi:10.1109/ACCESS.2020.3005762.

[28]   Song, Ch. H., Kim, D. H., Kim, K. Ch., "*Design of a novel IPMSM bridge for torque ripple reduct*ion", IEEE Trans. Magn., Vol. 57, pp. 1-4, Feb. 2021, doi:10.1109/TMAG.2020.3016985.

[29]   Hu, Y., Zhu, S., Xu, L., Jiang, B., "*Reduction of torque ripple and rotor eddy current losses by closed slots design in a high-speed PMSM for EHA applications*", IEEE Trans. Magn., Vol. 58, pp. 1-6, Feb. 2022, doi:10.1109/TMAG.2021.3083664.

[30]   Zhu, Sh., Hu, Y., Liu, Ch., Jiang, B., "*Shaping of the air gap in a V-typed IPMSM for compressed-air system applicati*ons", IEEE Trans. Magn., Vol. 57, pp. 1-5, Feb. 2021, doi:10.1109/TMAG.2020.3034152.

[31]   Abdos, A. A., Moazzen M. E., Gholamian S. A., Hosseini, S. M., "*Design Optimization, Voltage Quality, and Torque Ripple Improvement of an Outer Rotor Permanent Magnet Generator for Direct-Drive Wind Turbines Application*", Energy: Engineering & Management; Vol. 12, pp. 1-3, 2022, doi: 10.22052/12.3.52.

[32]   Hanselman, D. C., "Brushless permanent magnet motor design", 2nd ed. Cranston, RI, USA: The Writers' Collective, 2003.